Slidequake Generation versus Viscous Creep at Softrock-landslides: Synopsis of Three Different Scenarios at Slumgullion Landslide, Heumoes Slope, and Super-Sauze Mudslide

Marco Walter[1,2], Joan Gomberg[3], William Schulz[4], Paul Bodin[5] and Manfred Joswig[2]
[1]Seismic Solutions, Mettinger Strasse 103-105, 73728 Esslingen, Germany
Email: Marco.Walter@seismicsolutions.de
[2]University of Stuttgart, Institute for Geophysics, Azenbergstrasse 16, 70174 Stuttgart, Germany
[3]U.S. Geological Survey, University of Washington, Dept. of Earth & Space Sciences, Box 351310, Seattle, WA 98195, U.S.A.
[4]U.S. Geological Survey, Box 25046, MS-966, Denver, CO 80225, U.S.A.
[5]University of Washington, Dept. of Earth & Space Sciences, Box 351310, Seattle, WA 98195, U.S.A.

Downloaded 12/23/16 to 130.79.10.204. Redistribution subject to SEG license or copyright; see Terms of Use at http://library.seg.org/

ABSTRACT

In this study, we describe conditions for slidequake generation at three different creeping softrock landslides: the Slumgullion landslide in the San Juan Mountains, Colorado, U.S., the Heumoes slope in the Austrian Alps, and the mudslide in Super-Sauze, French Alps. From a geomorphologic point of view, all three landslides are classified as creeping landslides with average velocities between centimeters to meters per year. Associating creep with viscous flow, and considering the largely saturated, clayey consistency of the slope body, one would not expect any brittle behavior. Thus, it came as a surprise that impulsive seismic signals indicative of shear fracture could be discovered by sensitive passive monitoring methods at all three slopes. These fracture signals occur in episodes, have similar signatures as small earthquakes, and could be located within the slide bodies, *i.e.*, are evidence of slidequakes.

Our investigations identified seismic and aseismic slip in each slide, with slidequakes focusing at significant bedrock structures or at lateral boundaries. Synoptic comparison of three scenarios underlines the importance of landslide-bedrock and landslide-lateral boundary interactions under gravitational loading and Mohr-Coulomb-type failure. Comparison to frictional and asperity models of crustal- and plate-scale boundaries may pave the way to a comprehensive understanding of slidequake generation, and future slope failure prediction.

Introduction

Slope-related failure by fracture processes with magnitudes of $M_L < 0.0$ has been observed on rockslides by classical seismological monitoring techniques. Gomberg *et al.* (1995) proposed the term 'slidequake', which describes the fracturing or stress relief of slope material by means of brittle failure. Slidequakes at rockslides were monitored by, *e.g.*, Roth *et al.* (2005) at the Aknes fjord in Norway, Brückl and Mertl (2006) in the Austrian Alps, Spillmann *et al.* (2007) in the Swiss Alps, for a rockslide by Helmstetter and Garambois (2010), and for a detaching rock column by Levy *et al.* (2011), both in the French Alps.

In contrast to the aforementioned studies, we present the analysis of slidequake generation at three landslides consisting of weak sediments: the Slumgullion landslide in Colorado, USA (Gomberg *et al.,* 1995, 2011), the Heumoes slope in the Austrian Alps (Walter and Joswig, 2008, 2009; Walter *et al.,* 2011), and the mudslide in Super-Sauze, French Alps (Walter *et al.,* 2009, 2012). As softrock landslides are usually classified geomorphically as creeping, the existence of measurable slidequakes caused by brittle deformation was not expected. Nevertheless, this study deals with the analysis of slidequakes observed at three different softrock landslides applying standard seismic instrumentation and signal processing tools, *e.g.*, dense seismic networks typically used for monitoring rockslides. The apparent contradiction of viscous creep and the coexistence of slidequakes on softrock landslides has relevance to crustal-scale tectonics, where aseismic creep coexists with earthquake and other seismic phenomena (Peng and Gomberg, 2010). This study provides new insights to the complexity of softrock-landslides behaviour, and helps to comprehensively understand the roles of interface structure and morphology on both scales.

 DOI: 10.2113/JEEG18.4.269

Downloaded 12/23/16 to 130.79.10.204. Redistribution subject to SEG license or copyright; see Terms of Use at http://library.seg.org/

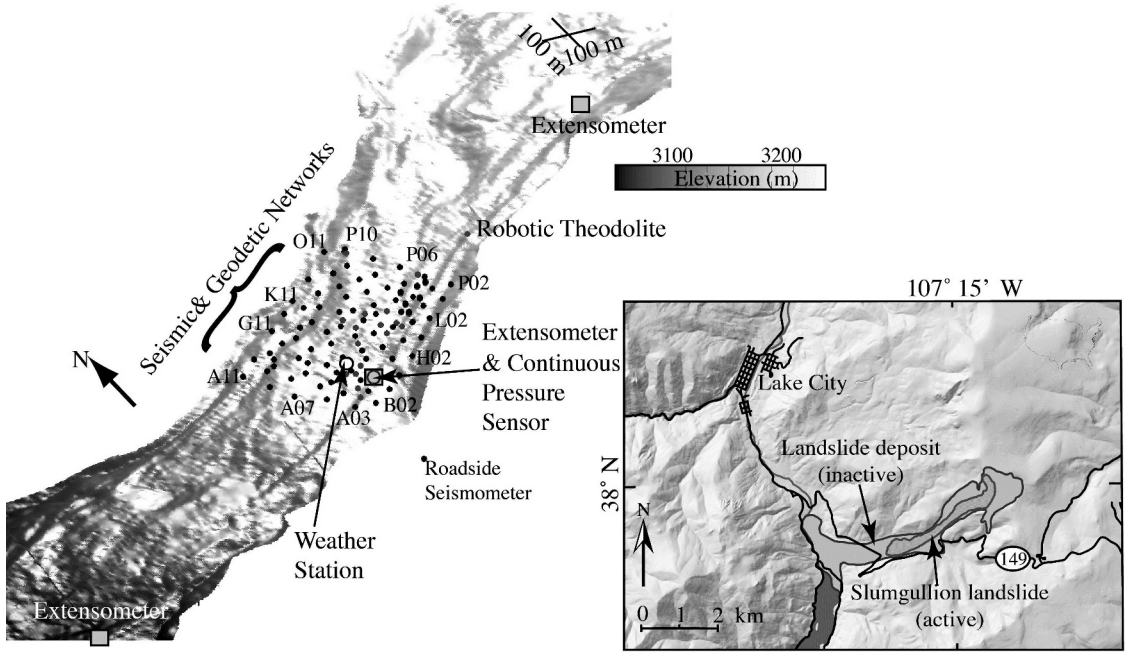

Figure 1. Set-up of Slumgullion landslide. Left: Projected view of the active landslide topography, with symbols showing locations of permanent extensometer pairs and pressure sensors, and seismic and geodetic instrumentation deployed during our field experiment. Prism locations used with a robotic theodolite were designed to measure aseismic deformation of the landslide surface. Seismographs were deployed on a grid, labeled (some shown) alphabetically going upslope and numerically across the slide. Right: Location map showing both the old and active landslide areas and the state highway (labeled '149') in the vicinity of the landslide.

Both the Slumgullion landslide and the Super-Sauze mudslide creep persistently at similar rates, have shallow and consistent groundwater levels, and have structures likely controlled by the basal topography. However, unlike the Slumgullion landslide that consists of volcanic deposits weathered to clayey sand and slides along bounding faults (Coe *et al.,* 2009; Schulz *et al.,* 2009a), the Super-Sauze mudslide is more like a granular flow (clayey schist that weathers to borderline coarse-fine soil), is younger (~50 yrs), and has some rockfalls and debris flows. The Heumoes slope also moves steadily, but more slowly (generally < 10 cm/yr) and is comprised of silty, loose scree and over-consolidated glacial till that slides on glacial till and calcareous marl, and thus likely exhibits more brittle behavior. In contrast to rockslides, the water content directly determines whether the material deforms as brittle failure or ductile-viscous deformation. Maquaire *et al.* (2003) investigated the shear strength properties of different black marls and determined the maximum moisture content for brittle deformation between 23% and 30% at different soil samples.

Gomberg *et al.* (1995, 2011) hypothesized that slidequake generation at the Slumgullion landslide might be analogous to that of tectonic faults with frictional behaviors ranging from stick-slip to steady creep. While most of the signals they observed originated outside the fastest-moving, monitored part of the slide, they inferred steady aseismic creep along the basal surface and stick-slip failure modulated by dilatancy along the slide-bounding strike-slip faults. In addition to impulsive slidequakes, Walter *et al.* (2009, 2012) observed energetic weaker signals with non-impulsive, reverberant, high frequency (relative to other signals on the slide) signatures clear at only one or a few sites at Super-Sauze. They inferred that these signals originated at the interfaces between the slide materials and bedrock where the latter formed crests, atop of which specific fissure structures often formed.

Study Areas

This section gives an outline of the geographical and geological settings of the landslides as well as a description of the specific slope deformation styles. Additionally, the respective seismic methods used for slidequake observation are explained in detail.

Slumgullion Landslide

The Slumgullion landslide (Fig. 1) is located in the San Juan Mountains of Colorado, U.S. It is composed of variably weathered Tertiary basalt, rhyolite and

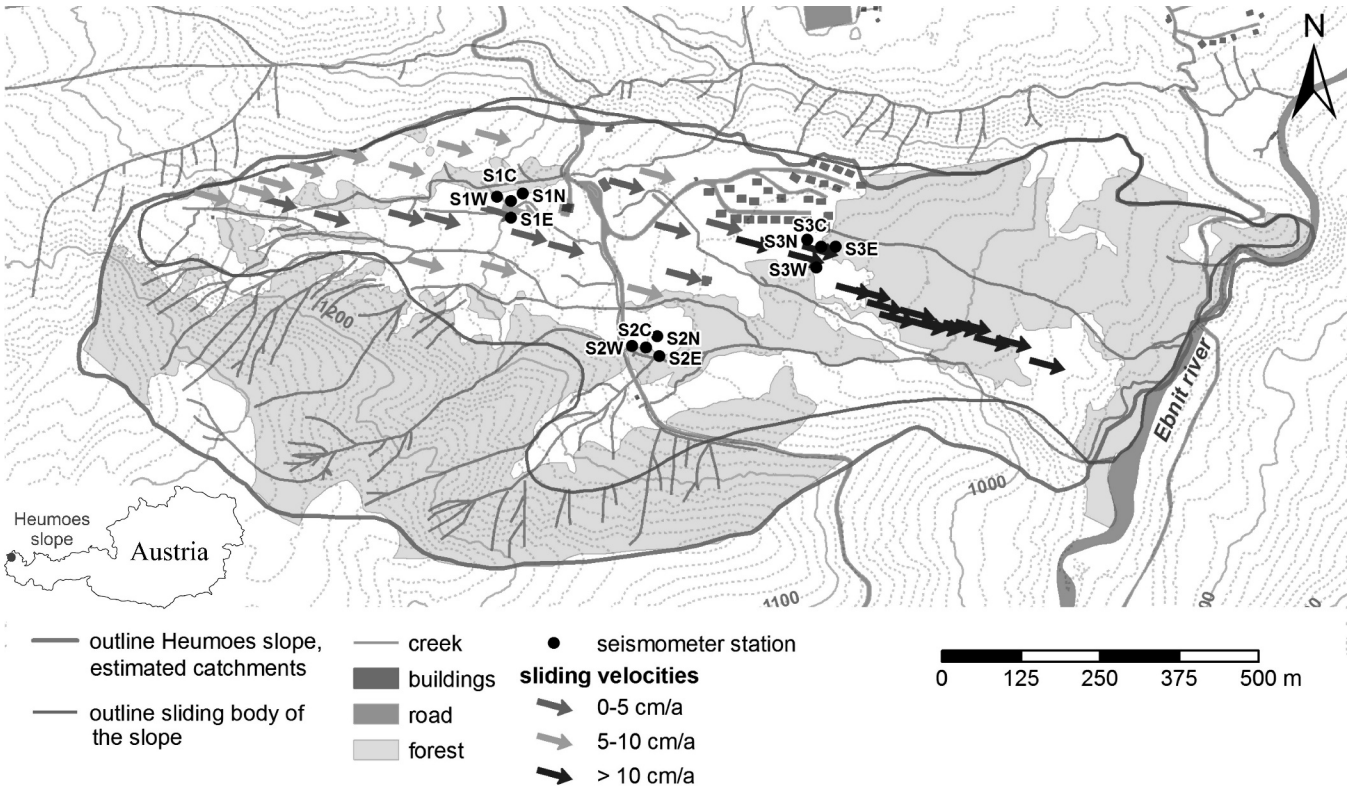

Figure 2. General set-up of the Heumoes slope, average sliding velocities (after Depenthal and Schmitt, 2003), and locations of installed seismometer stations of the permanent seismic network.

andesite units that have been highly modified by acid-sulfate hydrothermal alteration (Lipman, 1976; Diehl and Schuster, 1996) and weathered to clayey, silty sand. The landslide is situated within thicker landslide deposits comprised of similar material, although intact rock abuts the lateral margins of the active slide near its longitudinal center (Fig. 1). The landslide is 3.9-km long, averages about 300-m wide, and has an estimated average thickness of 13 m and volume of 20×10^6 m^3 (Parise and Guzzi, 1992).

The Slumgullion landslide moves persistently at rates of 0.5-2 cm/d (Fleming *et al.,* 1999; Coe *et al.,* 2003; Schulz *et al.,* 2009a) and appears to have done so for at least the past 300 yrs (Varnes and Savage, 1996). Pore-water pressures control landslide speed (Varnes and Savage, 1996; Coe *et al.,* 2003; Schulz *et al.,* 2009a), with significant rainfall or snowmelt causing landslide acceleration within hours and elevated speeds lasting for weeks-months. Shear-zone dilation and consequent pore-water pressure decrease appear to retard acceleration (Schulz *et al.,* 2009a), while onset of low atmospheric tides appears to trigger daily acceleration episodes (Schulz *et al.,* 2009b). Movement of Slumgullion occurs by translational sliding along clayey bounding faults, while many internal faults bound individual kinematic elements comprising the slide.

The field experiment, conducted August 18–26, 2009, involved deployment of a temporary seismic network and displacement measurement instrumentation spanning an ~450-m long section in the middle of the landslide where driving forces are greatest and surface velocities are the highest of anywhere on the landslide (Fig. 1; see Gomberg *et al.,* 2011 for details). An 88 short-period (2 Hz natural frequency) vertical seismometers array was deployed on a grid with inter-station spacings of 25–50 m extending across the entire slide width and just off it on both sides (Fig. 1). Slow, aseismic deformation was monitored in a variety of ways and a weather station within the array measured barometric pressure, temperature, wind speed, and rainfall, augmenting other permanent environmental monitoring gear (Fig. 1).

Heumoes Slope

The creeping Heumoes slope is located in the northern Alpine Upland, in the Vorarlberg Alps, Austria, around 25 km south of Bregenz (Fig. 2). The landslide extends 1,800 m in length and 600 m in width with elevations between 940 m (east) and 1,360 m (west). The unstable slope material has an average thickness of ~20 m (Lindenmaier *et al.,* 2005), and consists of very heterogeneous loamy scree and glacial till, which is mainly comprised of silty and clayey material as well as

Downloaded 12/23/16 to 130.79.10.204. Redistribution subject to SEG license or copyright; see Terms of Use at http://library.seg.org/

Downloaded 12/23/16 to 130.79.10.204. Redistribution subject to SEG license or copyright; see Terms of Use at http://library.seg.org/

glacial components of varying size from the surrounding bedrock. The hard rock basement consists of layered Upper Cretaceous marls. The movement of the Heumoes slope has been observed since the 1990s with various approaches. These investigations were mainly focused on the determination of geotechnical, hydrological and hydraulic relationships that lead to measurable displacements at the surface of a few centimeters per year. The Heumoes slope can be divided in three areas where different movement rates at the slope's surface were observed. The eastern part of the slope is characterized by the highest displacement rates of more than 10 cm/yr, while the western part of the landslide shows average displacements of up to 10 cm/yr. The most stable part of the Heumoes slope is located in the middle part, where average rates of up to 5 cm/yr were observed (Dependahl and Schmitt, 2003; Lindenmaier *et al.,* 2005; Fig. 2). A coupling of heavy rainfall and subsurface water dynamics was observed by Lindenmaier *et al.* (2005) and Wienhöfer et al. (2011), indicating that a rainfall-triggered movement of the Heumoes slope is most likely.

Several field campaigns were carried out between 2005 and 2008 to analyze slidequakes associated with the creeping movement of the Heumoes by deploying several small aperture seismic arrays. In these studies, a total of 39 slidequakes with magnitudes of $-2.2 \leq M_L \leq -0.7$ were recorded and located (Walter and Joswig, 2008; Walter *et al.,* 2011). The majority of events were located in the central section of the landslide, which displays lower surface displacement rates compared to its eastern part (Fig. 2). Since the eastern part of the slope shows the highest movement rates at the surface, one would expect to detect more events generated in this slope area. To understand and to investigate the spatio-temporal occurrence of slidequakes at the Heumoes slope, several permanent small-aperture seismic arrays were installed in July 2009 (Fig. 2). Each array consists of one 3-component and three 1-component short period seismometers with an aperture between 40 and 50 m. Data were recorded in continuous mode with a sampling rate of 400 Hz. The presented results are based on the data analysis between July 2009 and May 2011.

Super-Sauze Mudslide

The mudslide in Super-Sauze is located in the Barcelonnette Basin in the Southern French Maritime Alps, approximately between the cities of Gap and Nice (Fig. 3). The mudslide started to form in the 1960's and today it measures 850-m long with an elevation between 2,105 m (crown) and 1,740 m (toe). The unstable slope, with an estimated volume of 750,000 m^3, mainly consists of heterogeneous soft Jurassic black marls with a maximum thickness of ~20 m, and shows significant dynamic behavior with displacement velocities of more than 3 cm/d (Amitrano *et al.,* 2007). The observed average displacement rates of the mudslide vary: the highest movements can be observed in the mid-part of the slope and decrease in the toe direction to less than

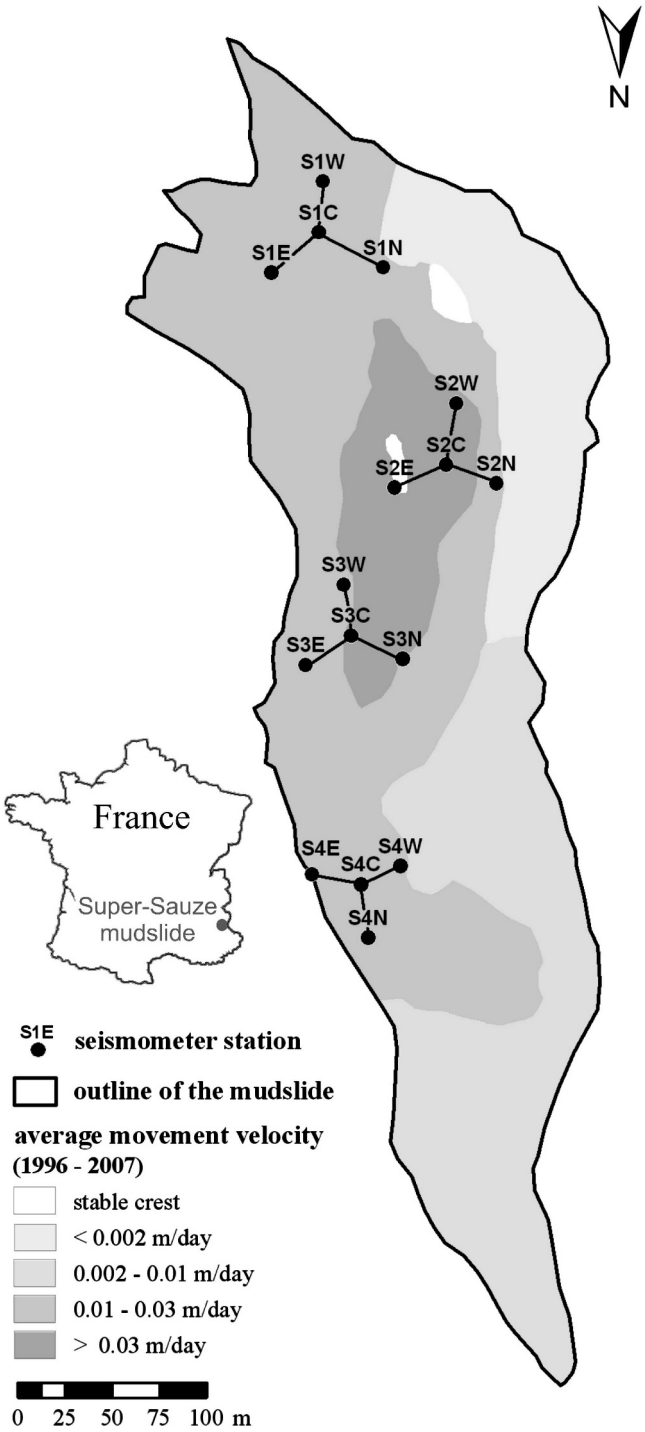

Figure 3. Location of the installed seismometer stations (black dots) and average movement velocity of the mudslide between 1997 and 2007 determined by Amitrano *et al.* (2007).

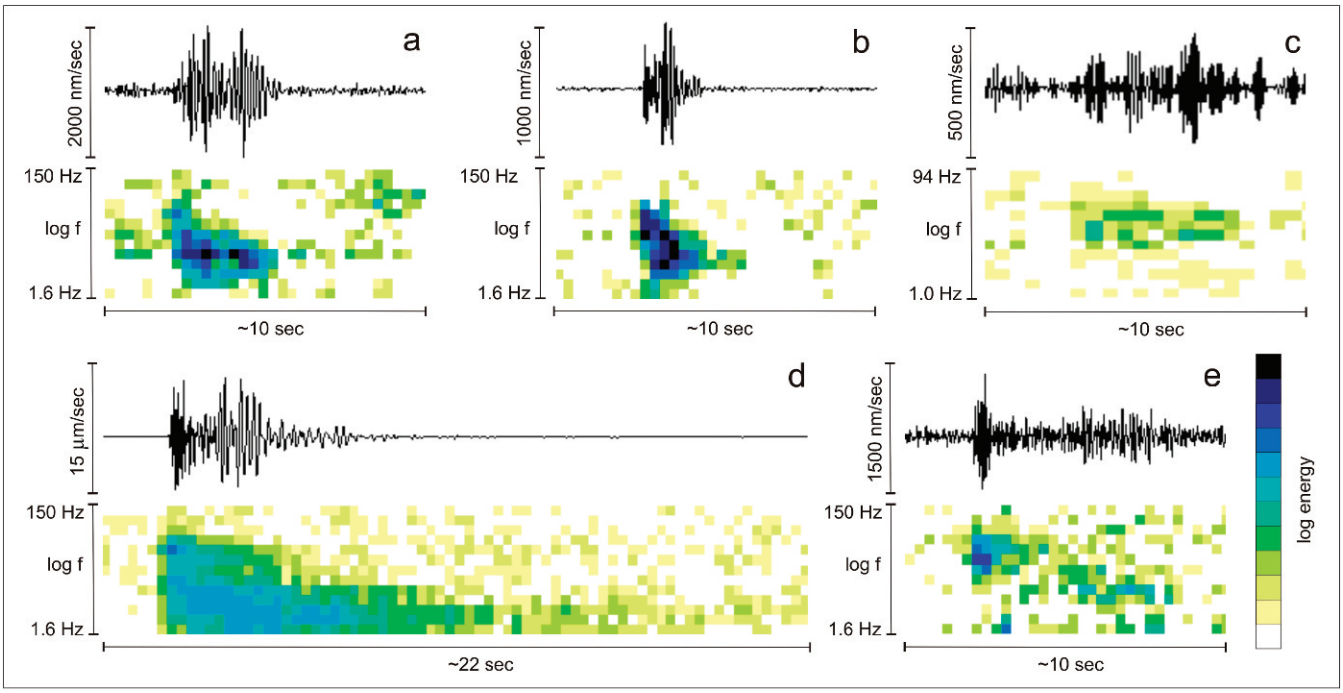

Figure 4. Comparison of typical seismograms and sonograms of observed slidequakes with local earthquakes. (a) Slidequake observed at Heumoes slope ($M_L = -1.4$ in ~180 m distance). (b) Slidequake observed in Super-Sauze ($M_L = -2.4$ in ~100 m distance). (c) Slidequake observed at Slumgullion. (d) Strong local earthquake ($M_L = 2.3$ in ~11 km distance). (e) Weak local earthquake ($M_L = 0.7$ in ~22 km distance). Note the different amplitude and frequency scales.

2 mm/day (Fig. 3). The influence of the bedrock topography to the stability of the slope was investigated by Maquaire *et al.* (2003). They inferred that heterogeneous movement of the entire mudslide is likely caused by stable buried in situ crests at the bedrock of the mudslide, with gullies between the crests channelizing the unstable material. Deformations of the entire mudslide are also directly influenced by its lateral boundaries (Maquaire *et al.,* 2003). Fissure patterns at the mudslide's surface were mapped by Niethammer *et al.* (2012) using UAV-based (Unmanned Aerial Vehicle) high-resolution remote sensing methods. They observed specific fissure patterns in slope areas that correlate with the locations of buried in situ bedrock crests and at lateral boundaries of the landslide.

In Super-Sauze, a field-campaign was carried out between 14th and 24th July 2008, where four small-aperture arrays were installed to monitor possible slidequake generation (Fig. 3). The aperture of the seismic arrays was setup similar to the Heumoes slope between 40 and 50 m. Data were also recorded continuously with a sampling rate of 400 Hz.

Slidequake Monitoring

The different seismic methods applied for slidequake detection, analysis and inferred models for slidequake generation are described in this chapter.

Applied Methods

Despite its remoteness from obvious natural and unnatural noise sources, a tremendous richness of seismic signals were recorded on the Slumgullion landslide. Details about the deployments, analyses, and interpretations of these signals may be found in Gomberg *et al.* (2011). The density of seismic stations deployed permitted some simple, albeit qualitative, assessments of signal origins. Almost all the seismic data were scanned visually. Many seismic signals were clearly not related to landslide deformation and based on arrival moveout times, no sources originated within the seismic network, although some could be attributed to sources along the edges of the seismic network. Location uncertainties for sources outside the network are inherently large, particularly because of the highly heterogeneous material and irregular topography of the Slumgullion landslide. For several event types, we applied quantitative source detection and location algorithms and used a variety of signal characteristics to glean clues about source type and location. To detect and measure some of the repeating signals, we employed a template cross-correlation approach. Event locations were estimated with two location algorithms, one using manually picked phase arrival times and a grid-search fitting between measured travel times and those calculated for a plane-layered medium (Gomberg *et al.,*

Downloaded 12/23/16 to 130.79.10.204. Redistribution subject to SEG license or copyright; see Terms of Use at http://library.seg.org/

Downloaded 12/23/16 to 130.79.10.204. Redistribution subject to SEG license or copyright; see Terms of Use at http://library.seg.org/

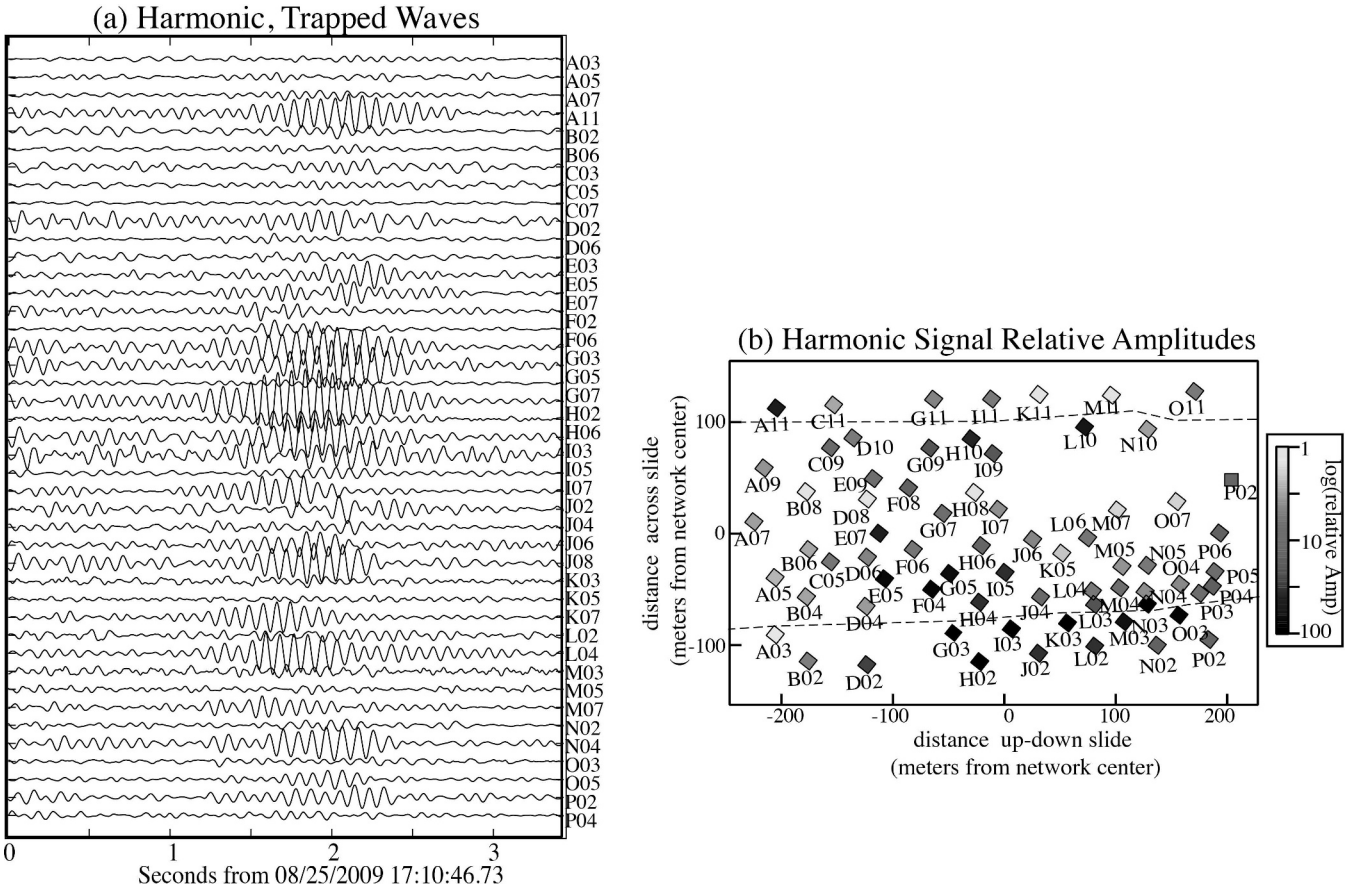

Figure 5. Sample waveforms and their amplitude distribution on the Slumgullion landslide. (a) Example of harmonic signals recorded at the sites with the best signal-to-noise ratios. (b) Map of the log of maximum harmonic signal amplitudes showing distribution highly peaked around the side-bounding fault, as expected for trapped waves.

1990). The other algorithm was a beam-forming approach developed for a landslide study elsewhere (see Lacroix and Helmstetter, 2011). Magnitudes were not estimated for any of the sources studied.

The recorded data at the Heumoes slope and at the mudslide in Super-Sauze were processed using the software HypoLine, an interactive, graphical jackknife tool which displays the most plausible solution for low SNR (signal-to-noise ratio) signals, resolving the influence of individual parameters on the event-localization in real time (Joswig, 2008). The raw data were high-pass filtered above 5 Hz to eliminate anthropogenic noise and to increase the SNR. As it was assumed that brittle failure takes place within the soft rock sedimentary cover, a layer over a homogeneous half-space model was used for event location and delivered the highest location accuracy of calibration shots; a 3-D model was not used. Compared to the Slumgullion landslide, the recorded slidequakes at Heumoes slope and the mudslide in Super-Sauze could be located by the use of the software HypoLine. The source location allowed additionally the determination of their local magnitude M_L, which permitted inferences about source processes and the estimation of the dimension of rupture areas. Because of the sparse station distribution and the low thickness of the respective sediment body, the source depth could not be determined.

Results

As noted in the previous section, characterization of the variety of recorded signals required significant qualitative and quantitative examination and analysis. Diagnostic parameters estimated included apparent phase velocities to constrain locations, signal coherency to detect families of repeating or similar sources, pattern recognition techniques to detect low-SNR slidequakes, and a variety of location algorithms. Many of the slidequake signals have properties that are remarkably similar to those of earthquakes and other local tectonic fault slip events: a high-frequency P-phase up to ~80 Hz and low frequency S-phase up to ~30 Hz (Walter and

Downloaded 12/23/16 to 130.79.10.204. Redistribution subject to SEG license or copyright; see Terms of Use at http://library.seg.org/

Joswig, 2008; Walter *et al.,* 2009, 2012; Gomberg *et al.,* 2011; Fig. 4). Because of the shallow source depth of slidequakes, the signals show a prominent surface wave coda. Maximum signal amplitudes varied over two orders of magnitude and the dominant frequency contents ranged from 10 to more than 80 Hz on all three slides. Site-effects and scattering also were surprisingly strong and variable, over scales of tens of meters.

Figure 4 shows typical seismograms and sonograms of recorded slidequakes at Heumoes slope, Super-Sauze and Slumgullion landslide (Figs. 4(a–c)). The lack of clear dispersion for the slidequake signals recorded at the Slumgullion landslide likely reflects propagation differences. Similar spectral characteristics (a decrease in frequency with time) can be observed in signals from local earthquakes (Figs. 4(d) and 4(e)).

Slumgullion Landslide

Here we summarize the most well constrained class of seismic source studied on the Slumgullion landslide. Details may be found in Gomberg *et al.* (2011). The most thoroughly analyzed signals are ~3 sec duration, monochromatic wavepackets that repeated over 90 times during the monitoring period (Fig. 5(a)). We inferred that these are trapped waves generated by stick-slip events along the slide-bounding strike-slip faults (Fig. 6), with occurrence rates that are highest in synch with daytime increases in the landslide slip rate. Evidence supporting this source type includes energy focused at 11.9 Hz at all stations and without harmonics, amplitudes strongly peaked at the stations along the southern edge of the landslide (Fig. 5(b)), variable apparent velocities that increase with distance, and high stacked correlation coefficients for locations along the southern edge of the landslide. Gomberg *et al.* (2011) explained these events by appealing to a model proposed by Schulz *et al.* (2009b), in which slide-bounding strike-slip faults slip fastest during the daytime when atmospheric pressure is lowest. The daily modulation of surface pressures modulates fluid flow within the slide mass, decreasing its basal frictional strength when surface pressures are lowest and allowing the slide to speed up. Dilatant strengthening (Schulz *et al.,* 2009a) along the lateral slide-bounding faults during more rapid shearing leads to increased rates of brittle failure events and effectively puts the brakes on the slip and the cycle repeats.

Heumoes Slope

At Heumoes slope, a total of 121 slidequakes of magnitudes $-2.5 \leq M_L \leq -0.5$ were recorded and located during the field campaigns between 2005 and 2008 (39 events) and during the permanent seismic monitoring between July 2009 and May 2011 (82 events). The vast majority of events are clustered in

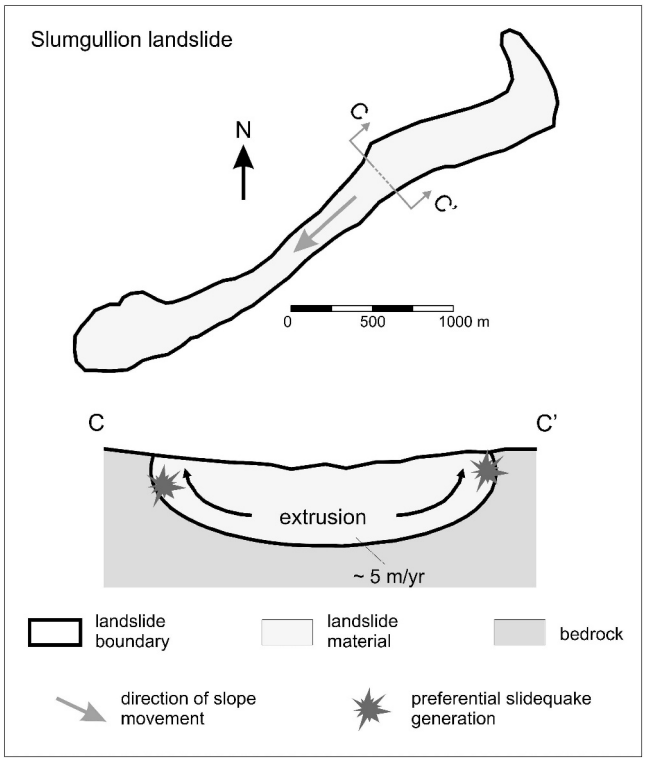

Figure 6. Schematic illustration of preferential slidequake generation at Slumgullion landslide (landslide and bedrock geometry modified after Fleming *et al.,* 1999).

the central section of the landslide, which is characterized by the lowest surface displacement rates (Fig. 7). Seismic refraction measurements across several profiles were carried out in 2006 to obtain detailed information about the bedrock geometry (Walter *et al.,* 2011). The active seismics revealed a significant upwarping of the bedrock in the mid-part of the slope. This bedrock elevation is oriented perpendicularly to the movement direction of the entire slope, and likely acts as a barrier and slows the surface displacement rates. Slidequakes occur at/near the interface between the barrier and slide material (Fig. 8). By contrast, in the most eastern part of the Heumoes slope sediments are thicker and lack barriers, and no slidequakes or any other seismic signals were observed. In addition, the slope material in the aseismic eastern part of the slope is always water saturated throughout, while the water saturation of the sliding material in the other parts of the Heumoes landslide varies seasonally in depth. Vertical sequences of saturated and unsaturated material are inferred in the center, seismogenic part of the slope, because of the generally low hydraulic conductivity (10^{-7} m/s; Lindenmaier *et al.,* 2005) of its clayey material that results in hydrology controlled by surface flow and along preferential water paths at depth rather than by

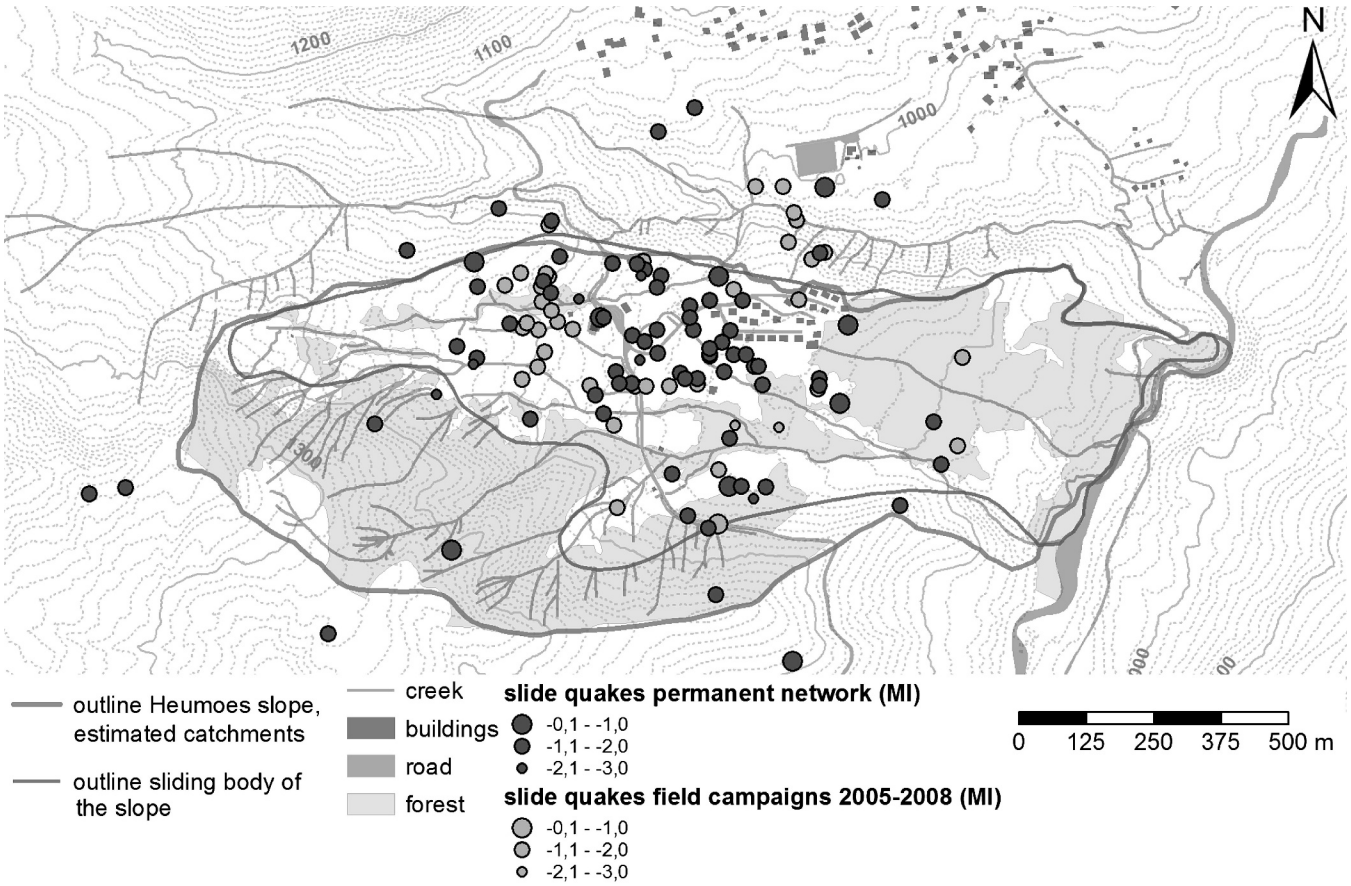

Figure 7. Locations and magnitudes of observed slidequakes at Heumoes slope during field campaigns between 2005 and 2008 (light grey dots) and the permanent seismic monitoring between July 2009 and May 2011 (dark grey dots).

infiltration processes (Lindenmaier *et al.,* 2005). We therefore assume that at Heumoes slope the observed slidequakes were generated in depth.

Super-Sauze Mudslide

At the mudslide in Super-Sauze, we detected and located 34 events with magnitudes between $-3.2 \leq M_L \leq -1.3$, again clustered in the mid-part of the slope (Fig. 9). Compared to the Heumoes slope, the ambient noise level at Super-Sauze is ~20 dB lower, which results in a lower detection threshold so a wider range of magnitudes were observed. A higher rate of slidequakes at Super-Sauze also likely reflects its faster velocity: 83 events in ~22 months at Heumoes slope compared to 34 events in 10 days at Super-Sauze.

At Super-Sauze the cluster of located slidequakes correlates well with the part of the slope showing the highest superficial displacement rates (Fig. 9). Fortunately, there exists an airborne picture from 1956, before the mudslide started to form, and illustrates the bedrock topography of the mudslide. This picture reveals crests that border the entire landslide and channelize the mudslide material in several gullies between. These crests are more or less oriented in the direction of slope movement. Figure 9 illustrates that the majority of observed slidequakes are not only generally related to the bedrock crests, but also occur in certain gullies with higher displacement rates. Figure 10 illustrates schematically the interpretation of preferential slidequake generation at the mudslide in Super-Sauze. Figures 9 and 10 show that the majority of slidequakes occurred at the boundaries of two gullies in the mid-part of the slope, which are characterized by higher average displacement rates of 11 m/yr, while fewer events were observed in the gullies moving at lower displacement rates.

Only the first meter of the landslide shows material deformation by brittle failure, when drying out in summertime. This is supported by the existence of remarkable fissure structures at the slope's surface (Niethammer *et al.,* 2012). Below the first meter, the landslide body is water saturated all the time. We therefore assume that, in contrast to the Heumoes slope, the observed slidequakes at Super-Sauze are generated within this top layer of the landslide.

Downloaded 12/23/16 to 130.79.10.204. Redistribution subject to SEG license or copyright; see Terms of Use at http://library.seg.org/

Downloaded 12/23/16 to 130.79.10.204. Redistribution subject to SEG license or copyright; see Terms of Use at http://library.seg.org/

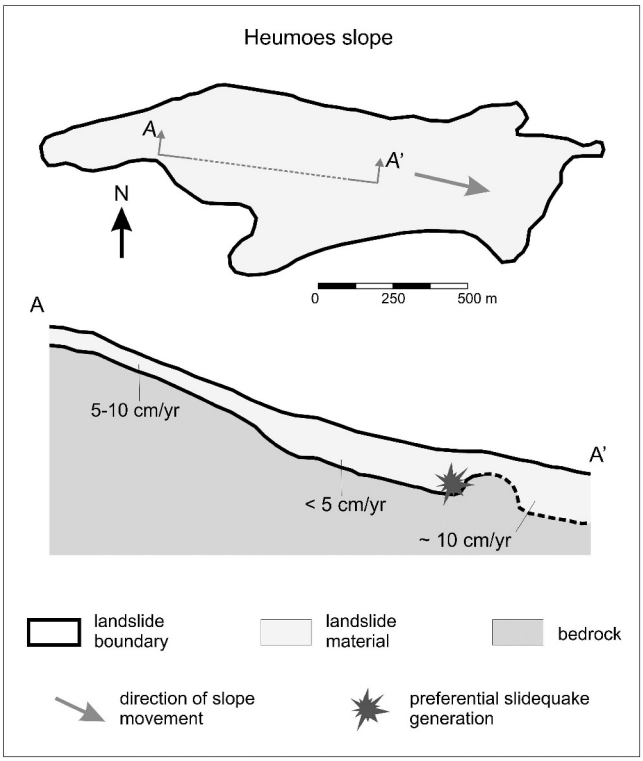

Figure 8. Schematic illustration of preferential slidequake generation at Heumoes slope (landslide and bedrock geometry modified after Walter *et al.*, 2011).

Discussion

The rates and manifestations of deformation are indicative of the underlying processes, *e.g.*, at Super-Sauze aseismic viscous creep likely occurs in areas of lower displacement rates and brittle failure manifests as slidequakes where rates are higher. This dependence of deformation mode on loading rate may be similar to that inferred for ascending magma, in which fast-rising magma deformed brittle and generated earthquakes, while slow-rising magma is characterized by ductile, aseismic deformations (*e.g.*, Tuffen *et al.,* 2003; Ichihara and Rubin, 2010). The observations at Super-Sauze support this hypothesis of a relationship between loading rate and slidequake generation. However, rate alone does not determine the dominant deformation mechanism since at the Heumoes slope slidequakes cluster where deformation rates are lowest.

At Super-Sauze slidequakes are most common along lateral boundaries and along the boundaries of crests of bedrock (Walter *et al.,* 2008, 2012). Brittle deformation is more likely when sedimentary or softrock materials are less saturated, with viscous creep becoming more probable as saturation increases (*e.g.*, Maquaire *et al.,* 2003). The lateral boundaries and significant bedrock structures at Heumoes slope and at Super-Sauze act as barriers along which slope material becomes more compressed, perhaps promoting draining, lower saturation and brittle failure.

The magnitudes of slidequakes observed at Heumoes slope and at Super-Sauze permits the estimation of possible source parameters. Assuming relationships derived by Wells and Coppersmith (1994) between moment magnitude (M_W) and rupture area dimensions and by Gibowitz *et al.* (1991) that $M_W \approx M_L$ for $M_W < -2.0$, the observed slidequakes at Heumoes slope and Super-Sauze with magnitudes of $-3.2 \leq M_L \leq -0.5$ correspond to rupture lengths in the range of several meters. The inferred fault plane dimensions and slip rates reasonably match slope extensions and creep rates.

At the Slumgullion landslide, the dilatant properties of the slide material also are key in determining the deformation modes. The continuous relocation of lateral boundary faults provides them with fresh material which, when sheared rapidly, dilates, strengthens and slows the motion. Thus, dilatancy strengthening when displacement rates are highest promotes brittle failure and slidequakes, and also keeps the motion in check. The apparently stable location of the basal surface has resulted in steady-state porosity, favoring aseismic slip.

At Super-Sauze, energetic weaker signals with non-impulsive, reverberant character were observed and located at the boundary between the emerging in situ crest and the mudslide material (Walter *et al.,* 2009, 2012). Similar tremor-like signals were also observed at the Slumgullion landslide (Gomberg *et al.,* 2011), but their source locations have not been determined. Tremor signals have been observed near tectonic faults in the transitional regime between frictionally locked and stably-sliding regions (Rubinstein *et al.,* 2010). The similarity of slope- and crustal-scale seismicity suggests that softrock-landslides may be a useful natural laboratory for testing predictions of specific mechanisms that control fault slip at all scales.

Conclusions

By applying passive seismic monitoring approaches at three different creeping softrock landslides, we were able to infer what conditions led to brittle failure, as evident in episodes of slidequakes along specific boundaries, and to aseismic creep. At the Slumgullion landslide, the majority of slidequakes occurred at the lateral boundaries of the landslide, while no events were detected along the basal surface (Fig. 6). Dilatancy-modulated motion along the lateral bounding, strike-slip fault systems is accompanied by stick-slip failure as the active fault strands continuously rearrange, but also keeps the long-term motion steady. This steady motion over many tens of years has likely led to basal

Downloaded 12/23/16 to 130.79.10.204. Redistribution subject to SEG license or copyright; see Terms of Use at http://library.seg.org/

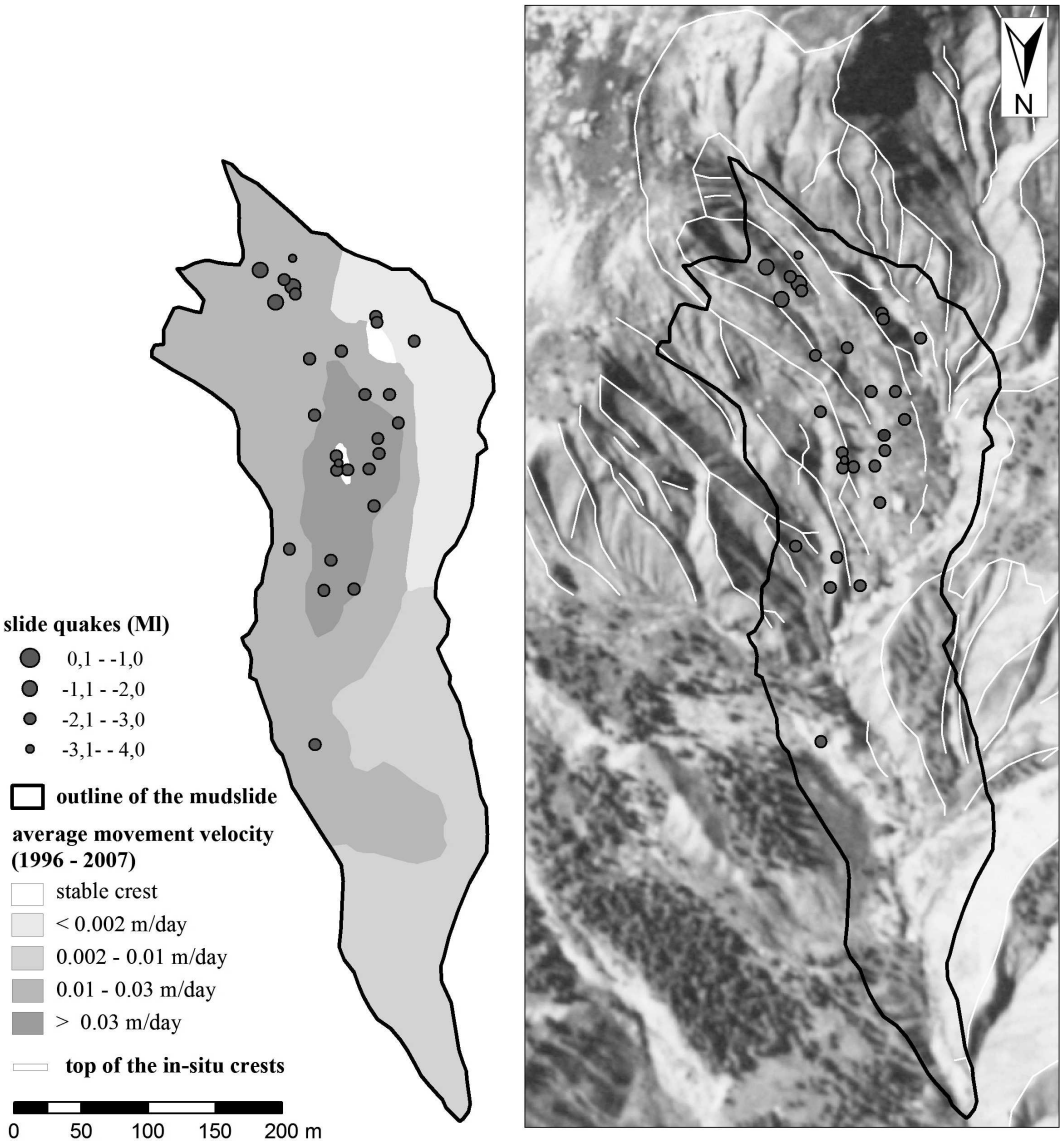

Figure 9. Locations of observed slidequakes at the mudslide in Super-Sauze. Left: Mapped on the average movement velocity of the mudslide (1997–2007) determined by Amitrano *et al.* (2007). Right: Mapped on an airborne picture from 1956, by courtesy of IGN (Institut Geographique National, Campaign F3139–3639). Highlighted are the tops of the in situ crests of the bedrock's topography.

morphology and porosity that have evolved to stable configurations, favoring steady aseismic sliding (Coe *et al.,* 2009; Gomberg *et al.,* 2011). At Heumoes slope, the slidequakes cluster in the slope area with the lowest surface displacement rates. A significant bedrock rise, oriented perpendicular to the direction of slope movement, divides the landslide geometry in two basins, and probably impedes motion, slows the slide, and leads to slidequakes (Fig. 8). At the Super-Sauze mudslide, the slidequakes are preferentially generated in its center where the deformation rates are highest. There, the slidequake generation is directly linked to in situ bedrock crests that border several gullies oriented in line with the direction of the entire slope movement (Fig. 10). The synoptic comparison of these three different environments of slidequake observations at softrock landslides provides new explanations for slidequake generation. Regardless of the specific observation of the respective landslide, the slidequake generation is generally linked to geometric or rheological heterogeneities along the boundaries between the slide material and the bedrock and/or along lateral boundary faults; these barriers seem to play key roles in slope deformations.

Downloaded 12/23/16 to 130.79.10.204. Redistribution subject to SEG license or copyright; see Terms of Use at http://library.seg.org/

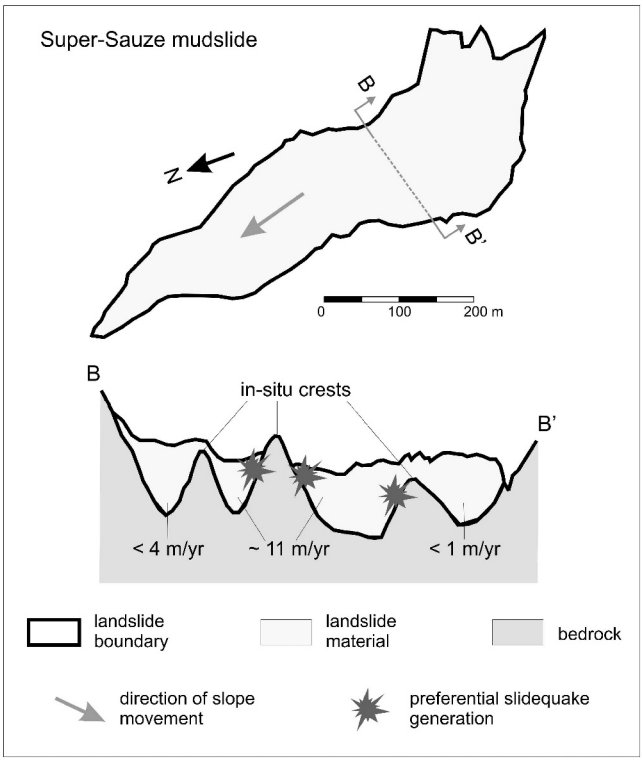

Figure 10. Schematic illustration of preferential slidequake generation at Super-Sauze (landslide and bedrock geometry modified after Malet *et al.*, 2005).

Acknowledgments

The authors thank Jason Kean for his contributions and the USGS's Venture Capital program for providing support for the Slumgullion study. We are thankful to the German Research Foundation (DFG) for their financial support for the studies at Heumoes slope and in Super-Sauze within the research unit FOR-581.

References

Amitrano, D., Gaffet, S., Malet, J.-P., and Maquaire, O., 2007, Understanding mudslides through micro-seismic monitoring: The Super-Sauze (South-East French Alps) case study: Bulletin de la Société Géologique de France, **178**(2) 149–157.

Beroza, G.C., and Ide, S., 2011, Slow earthquakes and nonvolcanic tremor: Annual Review of Earth and Planetary Sciences, **39**, 271–296.

Brückl, E., and Mertl, S., 2006, Seismic monitoring of deep-seated mass movements: Proceedings of INTERPRAEVENT International Symposium "Disaster Mitigation of Debris Flows, Slope Failures and Landslides", Universal Academy Press, Inc., Tokyo, Japan, 571–580.

Coe, J.A., Ellis, W.L., Godt, J.W., Savage, W.Z., Savage, J.E., Michael, J.A., Kibler, J.D., Powers, P.S., Lidke, D.J., and Debray, S., 2003, Seasonal movement of the Slumgullion landslide determined from Global Positioning System surveys and field instrumentation, July 1998-March 2002: Engineering Geology, **68**, 67–101.

Coe, J.A., McKenna, J.P., Godt, J.W., and Baum, R.L., 2009, Basal-topographic control of stationary ponds on a continuously moving landslide: Earth Surface Processes and Landforms, **34**, 264–279.

Depenthal, C., and Schmitt, G., 2003, Monitoring of a landslide in Vorarlberg/Austria: *in* Proceedings 11th International FIG Symposium on Deformation Measurements (Publication No. 2). Santorini (Thera) Island, Greece, Stiros, S. and Pytharouli, S. (eds.), Geodesy and Geodetic Applications Lab. Dept. of Civil Engineering, Patras University, 289–295.

Diehl, S.F., and Schuster, R.L., 1996, Preliminary geologic map and alteration mineralogy of the main scarp of the Slumgullion landslide: *in* The Slumgullion earth flow: A large-scale natural laboratory, Varnes, D.J. and Savage, W.Z. (eds.), U.S. Geological Survey Bulletin, **2130**, 13–19.

Fleming, R.W., Baum, R.L., and Giardino, M., 1999, Map and description of the active part of the Slumgullion landslide, Hinsdale County, Colorado: U.S. Geological Survey Geologic Investigation Series I-2672, scale 1:1,000, 36 pp.

Gibowicz, S.J., Young, R.P., Talebi, S., and Rawlence, D.J., 1991, Source parameters of seismic events at the underground research laboratory in Manitoba, Canada: Scaling relations for events with moment magnitude smaller than -2: Bulletin of the Seismological Society of America, **81**(4) 1157–1182.

Gomberg, J., Shedlock, K., and Roecker, S., 1990, The effect of S-wave arrival times on the accuracy of hypocenter estimation: Bulletin of the Seismological Society of America, **80**, 1605–1628.

Gomberg, J., Bodin, P., Savage, W., and Jackson, M.E., 1995, Landslide faults and tectonic faults, analogs?: The Slumgullion earthflow, Colorado: Geology, **23**(1) 41–44.

Gomberg, J., Schulz, W., Bodin, P., and Kean, J., 2011, Seismic and geodetic signatures of fault slip at the Slumgullion Landslide Natural Laboratory: Journal of Geophysical Research, **116**, B09404.

Helmstetter, A., and Garambois, S., 2010, Seismic monitoring of Séchilienne rockslide (French Alps): Analysis of seismic signals and their correlation with rainfalls: Journal of Geophysical Research, **15**(F3) F03016.

Ichihara, M., and Rubin, M.B., 2010, Brittleness of fracture in flowing magma: Journal of Geophysical Research, **115**, B12202.

Joswig, M., 2008, Nanoseismic monitoring fills the gap between microseismic networks and passive seismic: First Break, **26**, 121–128.

Lacroix, P., and Helmstetter, A., 2011, Location of seismic signals associated with microearthquakes and rockfalls on the Sechilienne Landslide, French Alps: Bulletin of the Seismological Society of America, **101**, 341–353.

Levy, C., Jongmans, D., and Baillet, L., 2011, Analysis of seismic signals recorded on a prone-to-fall rock column

(Vercors massif, French Alps): Geophysical Journal International, **186**(1) 296–310.

Lindenmaier, F., Zehe, E., Dittfurth, A., and Ihringer, J., 2005, Process identification at a slow-moving landslide in the Vorarlberg Alps: Hydrological Processes, **19**, 1635–1651.

Lipman, P.W., 1976, Geologic map of the Lake City caldera area, western San Juan Mountains, southwestern Colorado: U.S. Geological Survey Miscellaneous Investigation Series Map I-962, scale 1:48,000.

Malet, J.-P., van Asch, Th.W.J., van Beek, R., and Maquaire, O., 2005, Forecasting the behaviour of complex landslides with a spatially distributed hydrological model: Natural Hazards and Earth System Sciences, **5**(1) 71–85.

Maquaire, O., Malet, J.-P., Remaître, A., Locat, J., Klotz, S., and Guillon, J., 2003, Instability conditions of marly hillslopes: Towards landsliding or gullying? The case of the Barcelonnette Basin, South East France: Engineering Geology, **70**, 109–130.

Niethammer, U., James, M.R., Rothmund, S., Travelletti, J., and Joswig, M., 2012, UAV-based remote sensing of the Super-Sauze landslide: Evaluation and results: Engineering Geology, **128**, 2–11.

Parise, M., and Guzzi, R., 1992, Volume and shape of the active and inactive parts of the Slumgullion landslide, Hinsdale County, Colorado: U.S. Geological Survey Open-File Report 92–216, 29 pp.

Peng, Z., and Gomberg, J., 2010, An integrated perspective of the continuum between earthquakes and slow-slip phenomena: Nature Geosciences, **3**, 599–607.

Roth, M., Dietrich, M., Blikra, L.H., and Lecomte, I., 2005, Seismic monitoring of the unstable rock slope at Åknes, Norway: NORSAR, Report for the International Centre for Geohazards.

Rubinstein, J.L., Shelly, D.R., and Ellsworth, W.L., 2010, Non-volcanic tremor: A window into the roots of fault zones: *in* New Frontiers in Integrated Solid Earth Sciences, Cloetingh, S., and Negendank, J. (eds.), 287–314.

Schulz, W.H., McKenna, J.P., Biavati, G., and Kibler, J.D., 2009a, Relations between hydrology and velocity of a continuously moving landslide – evidence of pore-pressure feedback regulating landslide motion?: Landslides, **6**, 181–190.

Schulz, W.H., Kean, J.W., and Wang, G., 2009b, Landslide movement in southwest Colorado triggered by atmospheric tides: Nature Geoscience, **2**(12) 863–866.

Spillmann, T., Maurer, H., Green, A.G., Heincke, B., Willenberg, H., and Husen, S., 2007, Microseismic investigations of an unstable mountain slope in the Swiss Alps: Journal of Geophysical Research, **112**, B07301.

Tuffen, H., Dingwell, D.B., and Pinkerton, H., 2003, Repeated fracture and healing of silicic magma generate flow banding and earthquakes?: Geology, **31**, 1089–1092.

Varnes, D.J., and Savage, W.Z. (eds.), 1996, The Slumgullion earth flow: A large-scale natural laboratory, U.S. Geological Survey Bulletin, **2130**, 95 pp.

Vidale, J.E., and Houston, H., 2012, Slow slip: A new kind of earthquake: Physics Today, **65**(1) 38–43.

Walter, M., and Joswig, M., 2008, Seismic monitoring of fracture processes generated by a creeping landslide in the Vorarlberg Alps: First Break, **26**, 131–135.

Walter, M., Niethammer, U., Rothmund, S., and Joswig, M., 2009, Joint analysis of the Super-Sauze (French Alps) mudslide by nanoseismic monitoring and UAV-based remote sensing: First Break, **27**(8) 75–82.

Walter, M., and Joswig, M., 2009, Seismic characterization of slope dynamics caused by softrock-landslides: The Super-Sauze case study: *in* Proceedings of the International Conference on Landslide Processes: from geomorphologic mapping to dynamic modelling, Malet, J.-P., Remaître, A., and Boogard, T. (eds.), Strasbourg, CERG Editions, 215–220.

Walter, M., Walser, M., and Joswig, M., 2011, Mapping rainfall-triggered slidequakes and seismic landslide-volume estimation at Heumoes slope: Vadose Zone Journal, **10**(2) 487–495.

Walter, M., Arnhardt, C., and Joswig, M., 2012, Seismic monitoring of rockfalls, slide quakes, and fissure development at the Super-Sauze mudslide, French Alps: Engineering Geology, **128**, 12–22.

Wells, D.L., and Coppersmith, K.J., 1994, New empirical relationships among magnitude, rupture length, rupture width, rupture area, and surface displacement: Bulletin of the Seismological Society of America, **84**(4) 974–1002.

Wienhöfer, J., Lindenmaier, F., and Zehe, E., 2011, Challenges in understanding the hydrologic controls on the mobility of slow-moving landslides: Vadose Zone Journal, **10**(2) 496–511.

Downloaded 12/23/16 to 130.79.10.204. Redistribution subject to SEG license or copyright; see Terms of Use at http://library.seg.org/